Journal of Environmental Monitoring

Dynamic Article Links

Cite this: *J. Environ. Monit.*, 2011, **13**, 1212

www.rsc.org/jem

PAPER

Challenges for physical characterization of silver nanoparticles under pristine and environmentally relevant conditions†

Robert I. MacCuspie,*[a] Kim Rogers,*[b] Manomita Patra,[b] Zhiyong Suo,[b] Andrew J. Allen,[a] Matthew N. Martin[ac] and Vincent A. Hackley[a]

Received 11th January 2011, Accepted 22nd February 2011
DOI: 10.1039/c1em10024f

The reported size distribution of silver nanoparticles (AgNPs) is strongly affected by the underlying measurement method, agglomeration state, and dispersion conditions. A selection of AgNP materials with vendor-reported diameters ranging from 1 nm to 100 nm, various size distributions, and biocompatible capping agents including citrate, starch and polyvinylpyrrolidone were studied. AgNPs were diluted with either deionized water, moderately hard reconstituted water, or moderately hard reconstituted water containing natural organic matter. Rigorous physico-chemical characterization by consensus methods and protocols where available enables an understanding of how the underlying measurement method impacts the reported size measurements, which in turn provides a more complete understanding of the state (size, size distribution, agglomeration, *etc.*) of the AgNPs with respect to the dispersion conditions. An approach to developing routine screening is also presented.

Introduction

A variety of silver compounds and colloidal suspensions of silver (typically 15 nm to 500 nm) have been used throughout history for their bactericidal and fungicidal properties.[1] As a result of technological advances, engineered silver nanoparticles (AgNPs) of uniform size, shape and surface characteristics are becoming widespread for use as antibacterial agents (both in suspensions and as surface coating materials). The proliferation of these materials is also attracting attention because of their use in consumer products[2] and basic research,[3,4] and prompting increased regulatory and public interest in assessing whether or not any novel environmental, health and safety (EHS) risks are posed.[5–8] Moreover, the existence of naturally occurring colloidal AgNPs in the environment has been reported, both in the mid 1990's,[9] well before the recent surge in consumer products containing AgNPs, and recently in mining effluents in less-developed regions unlikely to have widespread use of AgNP-containing products.[10]

AgNPs are commercially available in size ranges from 1 nm to 100 nm and are typically surface modified with capping agents such as citrate, starch or polyvinylpyrrolidone (PVP). Although aqueous AgNP suspensions are often monodisperse when purchased from commercial sources, their agglomeration can be induced or inhibited by ionic strength, specific cations and the presence of biological molecules or natural organic matter (NOM).[11–13] Because the agglomeration state of AgNPs can also significantly affect transport and biological activity,[14] one of the current uncertainties with respect to investigating the nanoEHS effects and behavior of AgNPs is the variability in size

[a]*Material Measurement Laboratory, National Institute of Standards and Technology, Gaithersburg, MD, 20899-8520, USA. E-mail: robert.maccuspie@nist.gov; rogers.kim@epa.gov*
[b]*National Exposure Research Laboratory, Environmental Protection Agency, Las Vegas, NV, USA*
[c]*Materials Science and Engineering Department, University of Maryland, College Park, MD, USA*

† Electronic supplementary information (ESI) available: Detailed description of AFM image contrast adjustment for creating histograms and absorbance spectra over time for AgNPs in MHRW + I and MHRW + II. See DOI: 10.1039/c1em10024f

Environmental impact

Silver nanoparticles are reported to be used in the greatest number of consumer products containing nanomaterials, creating challenges for environmental risk assessment scientists and regulators. This work will facilitate intercomparison of sometimes conflicting environmental risk experiment results for nominally similar silver nanoparticles, elucidating the role that measurement methods and initial dispersion conditions have in the reported size distributions of materials. Recommendations are made that will enable easier comparisons across laboratories, and provide improved interpretation of experimental and environmental observations, with the aim of enabling more rapid science-based regulatory decisions.

distribution, polydispersity, and agglomeration, especially with respect to their introduction into environmentally relevant matrices. This is further compounded by the widely underappreciated differences in metrology across measurement techniques employed to report these physico-chemical properties. Indeed, while physico-chemical characterization of NPs by multiple techniques under relevant conditions has attracted attention in recent literature[15–17] and numerous lists suggesting minimum characterization reporting requirements of nanomaterials have been generated,[2] critical knowledge gaps still exist. Thus, this work specifically aims to identify potential pitfalls to avoid when reporting sizes and size distributions using several widely used physico-chemical characterization techniques, to explore the role of "stock" solution processing prior to measurement, and to develop rational approaches for comparison of the wide range of reported results. This work will enable more sophisticated re-interpretation of previous literature reports that may have initially appeared to be contradictory by reporting different nanoEHS results on nominally similar materials that were in fact significantly different. For example, the uncertainty associated with the aggregation of AgNPs and their interaction with NOM and inorganic compounds found in the environment can impact several areas of the source-to-outcome continuum used to determine risk.[18] Thus, comparison of measurement approaches and their underlying metrology, as applied to AgNPs, may better inform investigations designed to answer questions such as: (1) what are the major processes and/or properties that govern the environmental fate, transport, and transformation of manufactured nanomaterials? (2) how are these related to the physical and chemical properties of those materials? (3) what technologies exist, can be modified, or must be developed to detect and quantify manufactured nanomaterials in environmental media and biological samples?

Providing basic characterization parameters for commercial AgNPs in commonly used environmental test media will potentially be beneficial to scientists in this field.[19] Indeed, some preliminary reports using selected measurement techniques on a single type of AgNP can be found in the literature.[20] However, the work reported herein is unique in several ways: the range of AgNP materials and environmentally relevant dispersion conditions investigated, as well as the breadth of measurement techniques applied. Therefore, this work also aims to demonstrate one approach for identifying a routine screening assay to detect media-related changes in AgNP suspensions by relating precise, rigorous measurements of size and size distribution (*e.g.*, based on transmission electron microscopy (TEM), atomic force microscopy (AFM), or small angle X-ray scattering (SAXS)) to simple and inexpensive measurements with either proven techniques (based on optical properties, *e.g.*, by ultraviolet-visible spectroscopy (UV-vis) or dynamic light scattering (DLS)) or newer approaches (nanoparticle tracking analysis (NTA)) which may still suffer from reproducibility issues in their infancy.[21] This approach will be demonstrated on characterization data from a range of AgNP preparations with respect to size and size distribution in water, United States Environmental Protection Agency (EPA)-defined moderately hard reconstituted water (MHRW) and MHRW with Suwannee River Fulvic Acid Standard I or Humic Acid Standard II.

Experimental

AgNP materials

The vendor-reported nominal diameters are selected as the nominal diameters for AgNPs used throughout this paper. AgNPs were selected to provide as broad of a range as possible of sizes, capping agents, and powder/suspension states. Two separate batches were obtained, one for TEM, NTA, and UV-vis, and the second for AFM, USAXS, DLS, and UV-vis. Citrate-capped AgNPs were obtained from several sources, including 10 nm, 20 nm, and 100 nm from the NanoXact product line (Nanocomposix, San Diego, CA, USA); 20 nm, 40 nm, 60 nm, and 80 nm from the unconjugated silver colloids BBI product line (Ted Pella, Redding, CA, USA), and 20 nm from Microspheres-Nanospheres (Cold Spring, NY). Starch-capped (10 to 15 nm) AgNPs were obtained from Strem Chemicals (Newburyport, MA, USA). PVP-capped AgNPs 10 nm and 50 nm were obtained from the NanoXact product line (Nanocomposix, nominal, San Diego, CA, USA) and 10 nm, 30 to 50 nm, and 50 nm from NanoAmor (Houston, TX, USA). Oleic acid capped 30 to 50 nm AgNPs were obtained as powders from NanoAmor (Houston, TX, USA). AgNPs (1 to 10 nm) (no capping agent specified) were obtained from Vive Nano (Toronto, Canada). Stock dispersions of AgNPs received as powders were prepared by adding 1.0 mg of AgNP powder to 1.000 mL of deionized (DI) water and sonicating in a bath sonicator for 10 min. For selected measurements of the reconstituted AgNPs, the suspensions were first passed through a 0.45 μm polyvinylidene fluoride (PVDF) syringe filter. DI water (18.2 MΩ cm) was obtained from an Aqua Solutions (Jasper, GA, USA) Type I biological grade water purification system outfitted with an ultraviolet lamp to oxidize residual organics and a low relative molecular weight cut-off membrane, then passed through a 0.1 μm PVDF syringe filter before use. All AgNP suspensions were stored at 4 °C in the dark in their original containers, while powders were stored in the dark at ambient temperature. All AgNPs were characterized within 11 months of receipt from vendors, and frequently within 3 months of receipt.

Dispersion preparation

AgNPs were analyzed as-received, diluted with deionized (DI) water, diluted with EPA MHRW,[22] or MHRW plus Suwannee River Fulvic Acid Standard I or Suwannee River Humic Acid Standard II (1S101F and 2S101H, respectively, International Humic Substances Society, St Paul, MN, USA) at a NOM concentration of 10 μg mL^{-1}. AgNPs were added to diluents, shaken by hand for 2 s, then allowed to stand for at least 1 h before measurements began.

UV-vis spectroscopy

UV-vis spectra were collected on both Perkin Elmer (Waltham, MA, USA) Lambda 750 and Hewlett Packard (HP) Model 8453 spectrophotometers in UV-transparent disposable plastic semi-micro cuvettes (Brandtech, Inc., Essex, CT, USA) with a 1 cm path length, requiring 1 mL sample volumes. The Perkin Elmer spectrometer uses a split-beam configuration equipped with an 8 + 8 cell changer and water-jacketed temperature control;

measurements were performed at 25.0 ± 0.2 °C. The HP instrument has a single beam configuration and measurements were taken at 25 °C. Concentrated AgNP solutions were diluted such that the initial absorbance was approximately 1.0 at the surface plasmon resonance (SPR) absorbance peak wavelength (λ_{max}).

Dynamic light scattering (DLS)

The DLS methodology followed recommendations outlined in the NIST-Nanotechnology Characterization Laboratory (NIST-NCL) Assay Cascade protocol PCC-1.[23] DLS measurements were performed using a Malvern Instruments (Westborough, MA, USA) Zetasizer Nano in 173° backscatter mode. Sample preparation was performed in a particle-free hood. Disposable semi-micro cuvettes were cleaned and dried immediately before use. Measurements were performed at 20.0 ± 0.1 °C. The cumulants analysis algorithm was applied to obtain the Z_{avg} equivalent hydrodynamic diameter and the polydispersity index (PI). The PI is a metric for the width of the size dispersion, and an increase in PI is indicative of aggregation, agglomeration, or other processes that introduce size heterogeneity.

Nanoparticle tracking analysis (NTA)

Solutions were diluted to an approximate AgNP concentration range of 10^9 AgNPs per mL, and injected *via* a 1 mL disposable syringe into a Nanosight LM20 (Nanosight, Amesbury, UK) equipped with a 633 nm laser and low sensitivity detector. The liquid cell was cleaned by rinsing with filtered DI water between samples, and fresh DI water post-rinsing was checked to ensure no cross-contamination of AgNPs occurred. The optics were adjusted by finding the immobile area of diffraction from the laser beam, or so-called fingerprint, and moving the liquid cell so that the volume closest to the fingerprint without interferences was the volume observed. Camera settings were adjusted empirically by maximizing the brightness of the AgNPs while minimizing any background light. Videos were collected for 30 s. Post-collection analysis parameters were adjusted empirically to maximize the number of particles correctly identified by the proprietary software (NTA version 2.0) while simultaneously minimizing the number of noisy pixels incorrectly identified. As with most measurement techniques, incorrect use of the instrument can produce incorrect or misleading data. Thus, video analysis parameters including blur, detection threshold, gain, brightness, and number of completed tracks were adjusted independently and systematically to maximize the number of completed tracks obtained during a video analysis before reporting sizing results using those processing conditions.

Transmission electron microscopy (TEM)

NIST-NCL Assay Cascade protocol PCC-7 was broadly followed.[24] Briefly, amine-functionalized silicon TEM windows (Dune Sciences, Eugene, OR, USA) were immersed into a AgNP solution, incubated for 1.0 min, then rinsed by immersion into filtered DI water. Images were acquired at 300 kV using a Tecnai TEM (FEI, Hillsboro, OR, USA) with a 2k Gatan camera. The imaged structures were also analyzed by energy dispersive X-ray spectroscopy for elemental composition using an EDEX detector. At least 5 locations on the TEM window (grid) were examined, and between 50 and 90 images were recorded. Image J software was used for image analysis, freely available on the internet.[25,26] Sizes were measured by using the line distance measuring tool across the diameter of the AgNP, calibrated to the scale bar imprinted on the TEM.

Atomic force microscopy (AFM)

NIST-NCL Assay Cascade protocol PCC-6 was broadly followed.[27,28] Briefly, AFM samples were prepared by incubating 20 μL of AgNP dispersion on a 5 by 5 mm single side polished silicon wafer piece functionalized with 3-aminopropyldimethylethoxysilane (Gelest, Morrisville, PA, USA), referred to as AFM substrates. Measurements were performed using a Dimension 3100 AFM with a Nanoscope V controller (Bruker AXS, Santa Barbara, CA, USA) operated in intermittent contact or tapping mode, using an open-loop scanner. Cantilevers with a nominal spring constant of 7.4 N m^{-1} and a tip radius of curvature of less than 8 nm (NanoAndMore, Lady's Island, SC, USA) were used to collect all images. No less than 10 images were collected at arbitrary locations across a sample using an automated programmed-move routine to collect up to 100 images from up to 10 samples per session. One tip was used per session and then discarded. Figures shown are representative of all particles imaged. A subset of structures were analyzed using the cross-section analysis tool of the Nanoscope v7.20 software and manually selecting a point on the substrate surface and a point at the peak of the AgNP and recording the difference in Z-height between points. Image contrast for Z-height data was examined at two settings to ensure proper sizing of small and large AgNPs (see Fig. S1 and S2† for details).

Ultra small angle X-ray scattering (USAXS)

USAXS measurements were carried out at sectors 32-ID and 15-ID at the Advanced Photon Source (APS). The instrument is described in detail elsewhere.[29–31] Experiments were performed at ambient temperature (approximately 25 °C). For USAXS scans, a (0.4 × 0.4) mm monochromatic (energy = 10.5 keV, $\lambda = 0.118$ nm) incident X-ray beam was used. The scattering data were corrected for parasitic background scattering and for attenuation (using data from an aqueous buffer). See the ESI† (Fig. S3) for extended discussion on background subtraction in USAXS samples with low scattering intensity. The USAXS data, which are inherently slit-smeared perpendicular to the scanning direction, were absolute-calibrated with respect to the incident beam intensity according to first-principle methods,[31] and desmeared using the well-established Lake algorithm.[32] For measurements, approximately 0.3 mL of suspension was enclosed within a 1 mm thick liquid cell with polyamide film windows.

To obtain quantitative NP volume fraction size distributions the calibrated 1-D USAXS intensity data, $I(Q)$ *versus* Q (where $Q = (4\pi/\lambda)\sin\Theta$ is the magnitude of the scattering vector, λ is the X-ray wavelength and Θ is half of the scattering angle), were analyzed using an entropy maximization algorithm known as MaxEnt.[33] The USAXS data were reduced and analyzed (including implementation of MaxEnt) within the Irena 2

package of data evaluation and modeling macros for Igor Pro (Wavemetrics, Lake Oswego, OR, USA).[34]

Uncertainty reporting

The approach taken throughout this paper for reporting uncertainties is as follows. Error bars for TEM and AFM represent one standard deviation about the mean for all particles counted in a sample. The TEM and AFM error bars therefore represent the width of the distribution, and are not reflective of the uncertainty associated with determining the mean size. For DLS, the mean of five replicate Z_{avg} measurements under repeatability conditions is reported, with error bars of one standard deviation about the mean of the Z_{avg} values. The DLS error bars represent the repeatability of the DLS measurement (the ability to achieve the same measurement result consecutively), and do not indicate the width of the size distribution. For USAXS, an estimated measurement uncertainty of $\pm 10\%$ is assigned to all values reported, based on the previous experience measuring NIST gold NP reference materials RM8011, RM8012, and RM8013.[35–37] Again, this represents the USAXS uncertainty in the mean diameter, not a measure of the width of the size distribution.

Results and discussion

Role of handling on size and size distribution

Scientists wishing to test size-effect-based hypotheses require well-characterized size distributions, and desire the narrowest size distributions possible to achieve separation of size-dependent effects and the most meaningful conclusions. Yet, the conditions under which the materials are "initially" characterized can impact their reported size and size distributions, which are in turn used as the basis for interpretation of test results. Fig. 1 illustrates examples of the various points in material handling

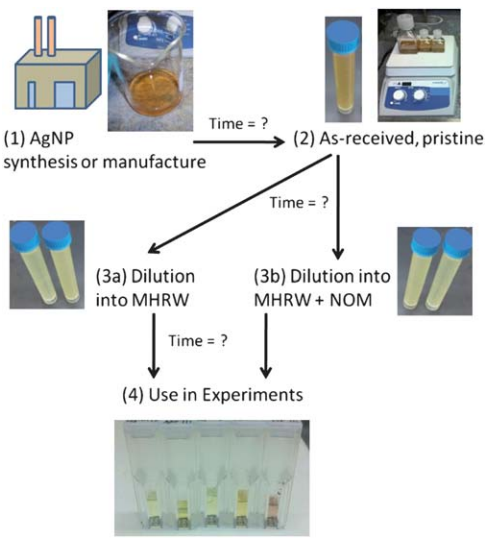

Fig. 1 Scheme illustrating some of the common points that measurements of "stock" AgNPs could take place. The variables of time between points and storage conditions can affect the stability and degradation kinetics of the AgNPs and thus the observed size and size distribution of the same lot of material.

where measurements can occur. To compare the strengths and weaknesses of each measurement technique, the AgNPs selected for this study were analyzed as received or diluted with DI water, which will be referred to as *pristine conditions* (Fig. 1, point 2), and diluted into MHRW (Fig. 1, point 3a), or MHRW with NOM Standard I or II (MHRW + I or MHRW + II, respectively) (Fig. 1, point 3b), discussed later, with the sizing results for each dispersion condition summarized in Tables 1, 2, and 3, respectively. Fig. 2 illustrates the differences between the reported nominal size (Fig. 1, point 1) and the observed mean size for the citrate-capped AgNPs for the pristine materials (Fig. 2a), and dilution into environmental media MHRW (Fig. 2b) or MHRW + I (Fig. 2c).

Pristine conditions

Fig. 2a illustrates the range of mean sizes that could potentially be reported for AgNPs under pristine conditions, and Table 1 details the numerical sizing results. The range of deviations from the nominal *vs.* measured line (dashed lines in Fig. 2) illustrates the complexity of intercomparing results. Among the citrate- and PVP-capped AgNPs from various sources, certain trends were noted. For example, Fig. 3 provides the size distributions for the citrate-capped AgNPs under pristine conditions. Samples B–D (Fig. 3b–d, respectively), each nominally 20 nm, yield mean diameter measurements of 21.3 nm, 15.6 nm and 23.6 nm, respectively, by AFM, and 20.3 nm, 20.9 nm and 29.2 nm, respectively, by TEM (see Table 1 for uncertainties). Representative TEM and AFM images of Sample D are shown in Fig. 4a and b, respectively. These AgNPs yield mean hydrodynamic diameters of 35.1 nm, 50.0 nm and 30.8 nm, respectively, by DLS and mode measurements of 33.2 nm, 39.0 nm and 51.0 nm, respectively, by NTA (Table 1). An example size distribution of Sample D obtained from NTA based on over 100 completed tracks is shown in Fig. 4c. The dry-state measurements provided by AFM and TEM show mean diameter values that differed by less than 10 nm from the nominal reported values, whereas the measurements of average hydrodynamic diameter are larger by up to 30 nm, suggesting influence from surface coatings, a few large-sized outliers, and/or the presence of small agglomerates. Most of the citrate- or PVP-capped AgNPs that are greater than 20 nm follow these measurement method trends. For AgNPs nominally less than 20 nm (Samples A, I, J, M, and N), mean diameter measurements by AFM and TEM range from 7.9 nm to 12.4 nm and 3.6 nm to 52.0 nm, respectively. By contrast, mean hydrodynamic diameters measured by DLS and NTA range from 22.7 nm to 547 nm and 18.2 nm to 195 nm, respectively. The larger increases (greater than 300%) for the hydrodynamic diameter measurements of these AgNPs suggest the presence of AgNP agglomerates is common.

Environmental media

Measurements that show the greatest positive deviations from the sizes reported by the manufacturers involve hydrodynamic diameter values (measured by DLS and NTA) for AgNPs less than 20 nm. Deviations below the nominal *vs.* measured line were observed for AFM and USAXS measurements for AgNP with nominal diameters larger than 40 nm (Fig. 2a). When AgNPs

Table 1 Mean sizes of AgNPs under pristine conditions

Sample code	A	B	C	D	E	F	G	H	I	J	K	L	M	N	O
Nominal size/nm	10	20	20	20	40	60	80	100	10	10	50	50	1–10	10–15	30–50
Capping agent	citr.	citr.	citr.	citr.	citr.	citr.	citr.	citr.	PVP	PVP	PVP	PVP	unk.	starch	oleic acid
Form received	susp.	susp.	susp.	susp.	susp.	susp.	susp.	susp.	susp.	powd.	powd.	susp.	susp.	susp.	powd.
DLS mean Z_{avg}/nm	22.7	35.1	50.0	30.8	46.3	84.1	113.5	98.7	23.8	109.8	145.8	54.4	546.7	154.7	103.0
DLS SD[a]/nm	1.9	0.2	1.6	1.2	0.6	0.9	1.9	1.2	1.0	6.7	1.0	0.8	7.5	1.2	1.3
DLS mean PI	0.377	0.536	0.354	0.095	0.292	0.155	0.113	0.073	0.374	0.416	0.231	0.195	0.597	0.280	0.332
AFM mean height/nm	10.8	21.3	15.6	23.6	39.5	44.7	56.3	39.5	11.0	12.4	103.8	46.4	7.9	10.2	97.3
AFM SD[b]/nm[b]	2.2	3.9	6.5	4.6	18.9	37.5	50.4	40.6	2.2	19.9	91.8	8.5	5.4	5.4	69.9
AFM # NPs counted	107	102	100	100	131	71	44	100	102	100	102	100	102	106	105
NTA mean size[c]/nm[c]	28.8	44.0	48.2	28	74	106	111	130.2	54	—	—	39	194.6	18.2	75
NTA mode size/nm	20.0	33.2	39.0	51	62	87	106	122	26	—	—	30	21.8	16.6	38
# completed tracks	125	520	645	38	428	371	620	175	106	—	—	106	150	125	10.16
TEM mean size/nm	8.0	20.3	20.9	29.2	56.1	85.9	105.7	95.6	9.0	52.0	81.2	49.8	3.6	13.2	46.2
TEM SD[b]/nm	2.1	2.2	3.1	3.0	7.9	11.1	15.1	11.8	2.3	11.1	21.2	5.2	1.4	6.8	10.4
TEM # NPs counted	81	80	80	51	89	75	27	75	74	53	29	74	80	NA	82
USAXS mean size[d]/nm[d]	13.6	21.3	—	27.9	—	—	112.5	98.4	17.0	—	—	48.7	—	11.1	—
USAXS peak % of tot. vol. frac.[e]	99%	83%	—	71.2%	—	—	99.8%	100%	95%	—	—	100%	—	82%	—
USAXS tot. vol. frac. of All AgNPs ($\times 10^{-6}$)	2.34	1.90	—	6.86	—	—	4.29	0.25	0.38	—	—	2.23	—	33.2	—
UV-Vis λ_{max}/nm	389	403	401	407	432	489	471	486	394	432	—	424	430	408	423
UV-Vis peak abs[f]	3.42	2.2	—	0.96	0.54	0.3	0.19	0.75	76.16	—	—	79.42	17.64	3.86	7.38
Abs/mass Ag/μg mL^{-1}	0.17	0.11	—	0.048	0.027	0.015	0.094	0.037	0.076	—	—	0.079	0.012	0.24	0.008

[a] Measurements of AgNPs under pristine conditions (as-received or diluted into DI water). Nominal diameters or size ranges are provided by the source. [1] DLS Z_{avg} diameters are the mean of no less than five experiments performed under repeatability conditions, with one standard deviation uncertainty from the mean. [b] AFM heights and TEM diameters are the mean and one standard deviation of all AgNPs sized. [c] NTA mean and mode diameters are based on the number of AgNPs sized, or the number of completed tracks. [d] USAXS diameters are the mean size of the most significant size distribution peak, *i.e.* the peak with the greatest percentage of the total volume fraction of all AgNPs. [e] An estimated uncertainty of ±10% should be applied to all USAXS values. [f] UV-vis peak absorbance is calculated for the undiluted stock solution, using the dilution factor for solutions that provided measured absorbance values between 0.05 and 2.0. Dashes indicate no measurements using that technique were made on that sample.

Table 2 Mean sizes of AgNPs in MHRW. Sample codes and uncertainties follow same conventions in Table 1

Sample code	A	B	D	E	F	G	H	I	J	K	L	M	O
Nominal size/nm	10	20	20	40	60	80	100	10	10	50	50	1–10	30–50
DLS mean Z_{avg}/nm	33	49.9	39.0	51.6	90.8	121.0	195.9	146.2	227.7	111.0	43.8	126.9	251.1
DLS SD/nm	7.3	0.7	0.5	0.5	0.7	3.2	17.4	132.8	38.1	3.5	0.6	3.0	232.7
AFM mean height/nm	13.3	21.3	24.3	33.0	29.1	35.7	111.2	11.4	32.7	37.5	38.0	4.8	148.6
AFM SD/nm	4.6	5.3	4.6	23.0	24.8	44.1	22.6	4.0	38.8	49.8	14.1	3.8	87.6
AFM # NPs counted	101	100	102	37	26	18	4	100	56	8	55	102	82
NTA mean size/nm	133	42	56	60	85	104	104	—	—	—	52	62.7	131
NTA mode size/nm	20	52	53	56	81	100	97	—	—	—	46	52.7	114
# Completed Tracks	40	1128	1829	1653	7	403	1134	—	—	—	1869	646	293

with nominal sizes in the range of 20 to 100 nm are suspended in MHRW, measurements of the hydrodynamic diameter by DLS and NTA typically increased above the nominal *vs.* measured line (Fig. 2b). For Sample O, oleic acid-capped nominally 30 to 50 nm AgNPs, diameter values measured by DLS, NTA and AFM significantly increase (Fig. 2b). The addition of NOM in the form of Suwannee River Fulvic Acid Standard I (MHRW + I) nearly eliminates these deviations for AgNPs with average diameters larger than 20 nm, as measured by DLS (Fig. 2c), and reduces the deviation for Sample D (citrate-capped nominally 20 nm AgNPs, Fig. 5a).

The diameter of the AgNPs can be expected to differ somewhat depending on several factors, including the measurement technique, the thickness of the initial capping agent, and the thickness of the NOM layer sorbed onto the AgNPs. The capping agent and NOM density on the surface, and ability of NOM molecules to competitively displace the initial capping agent will also impact the observed size. Tables 2 and 3 summarize the observed sizes in MHRW and MHRW + I, respectively, in selected samples. Fig. 5 illustrates, for Sample D specifically, the impact of the measurement technique combined with measurement media or sample process history on the observed mean size. The size distribution results under pristine conditions (Fig. 5b) converge near a mode at 30 nm diameter. The AFM and DLS modal diameters do not vary much across the three media, although both the techniques revealed a broader size distribution in both MHRW (Fig. 5c) and MHRW + I (Fig. 5d). This broadening may be due to the formation of small agglomerates in MHRW, the adsorption of NOM, or dissolution of the AgNPs.

Molecules that sorb onto the AgNP surface can provide additional colloidal stability against charge screening through steric repulsive forces. This stability becomes evident comparing the results for AgNPs in MHRW and MHRW + I, and again by comparing citrate-capped and PVP-capped AgNPs (Tables 2 and 3, A and I). In MHRW, the presence of higher electrolyte levels leads to charge screening and a reduction of the Debye length, which causes the electrostatic repulsive forces to decrease significantly. Moreover, the AgNPs in MHRW + I are less stable over 72 h (Fig. 6a and S4–S14†) than AgNPs in MHRW with Humic Acid Standard II (MHRW + II) over 42 h (Fig. 6b and S15–S22†).

The results with Sample D in Fig. 6 illustrate the difference in the two NOM standards' abilities to stabilize single citrate-capped AgNPs and slow their agglomeration in MHRW. The decrease of the single AgNP SPR absorbance peak near 400 nm, and the appearance of a second absorbance peak at red-shifted wavelengths after several hours, indicates agglomerates are forming in solution. The agglomerate peak red-shifts in peak wavelength and absorbs more strongly with Fulvic Acid Standard I (Fig. 6a) compared to Humic Acid Standard II (Fig. 6b). These results suggest that both the type of NOM, as well as the length of time between dispersion preparation and characterization, are critical experimental factors to report alongside size distributions of "stock" AgNPs.

Powders *versus* suspensions

AgNPs received as aqueous suspensions more frequently exhibit narrow size distributions compared with powders that require a subsequent dispersion step. Indeed, the quality of dispersions formed from dry powders varies widely, depending upon many factors including those associated with the application of ultrasonic energy (*e.g.*, input power, temperature, geometry of the sonicator and solution vessel), the selection or inclusion of capping agents, and solution chemistry.[38] Recently, protocols addressing how to prepare[39] and report the preparation of these powders[40] have been published. There can also be temporal changes to the quality or stability of powder dispersions. For example, serial dilutions of a powder of PVP-capped AgNPs

Table 3 Mean sizes of AgNPs in MHRW + I. Sample codes and uncertainties follow conventions in Table 1

Sample code	A	B	D	E	F	G	H	I
Nominal size/nm	10	20	20	40	60	80	100	10
DLS mean Z_{avg}/nm	25.8	38.4	37.8	38.4	61.6	88.1	100.7	45.5
DLS SD/nm	0.5	1.5	1.6	1.3	0.8	1.1	1.2	22.9
DLS mean PI	0.289	0.471	0.294	0.267	0.209	0.168	0.069	0.214
AFM mean height/nm	9.6	16.3	19.0	8.7	12.2	12.2	17.8	9.0
AFM SD/nm	3	7.1	10.3	5.8	12.5	14	8.4	2.2
AFM # NPs counted	100	18	100	101	101	100	7	100

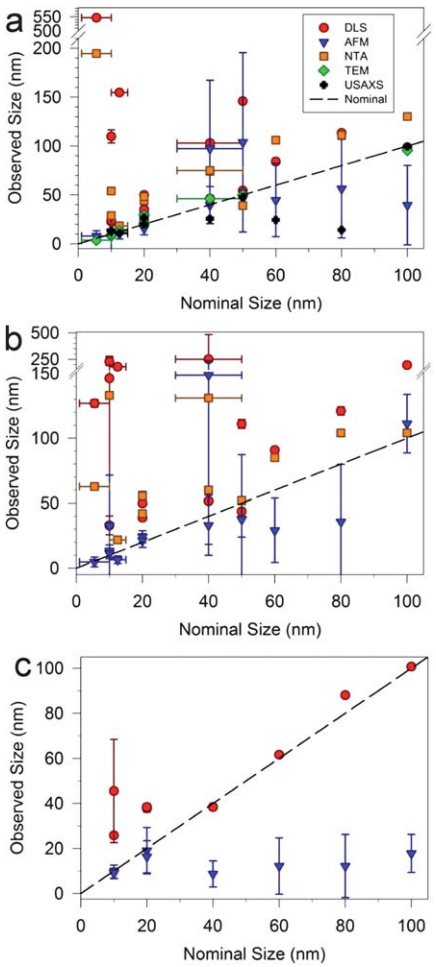

Fig. 2 Mean size by measurement technique plotted against the "nominal" size reported by the manufacturer for (a) pristine conditions, (b) dilution into MHRW, and (c) dilution into MHRW + NOM I. All panels use legend shown in (a). Vertical bars in observed size (*y*-axis) follow conventions described in the Experimental section, keeping in mind that error bars for different techniques have different meanings, from precision of the measurement to width of the distribution; refer to Tables 1–3 for values smaller than symbols. Horizontal bars in nominal size (*x*-axis) represent the range provided by the source, where appropriate.

dispersed into DI water were examined by collecting an absorbance spectrum every hour for 96 h (surface plots of the entire datasets are available in Fig. S23–S26†) after treatment in a bath sonicator and vortexing for approximately one min, this experiment reveals what might typically be reported for an absorbance spectra over the wavelength range of 300 to 800 nm. At longer wavelengths, a turnover to a broad absorbance that is nearly featureless occurs, suggesting the sample is a very polydisperse, significantly aggregated suspension that settles below the beam-path nearly completely (approximately 90% loss of absorbance) over a few days.

Measurement method impact on observed size distribution

Microscopy. The underlying metrology of the measurement techniques employed will impact the reported size and size distribution of the AgNPs. For example, microscopy-based techniques such as scanning electron microscopy (SEM), TEM, or AFM typically require dried samples fixed on a solid support, and the sample preparation method can impact the results considerably (*e.g.*, by producing artifacts of the drying process). NIST-NCL Assay Cascade protocols PCC-6 and PCC-7 provide further details on how to minimize these effects by either electrostatically or covalently attaching NPs in solution onto a solid imaging support and thereby mitigate drying-induced agglomeration.[24,27,41,42]

TEM provides greater contrast with increased atomic number elements. Thus, the Ag core of the AgNP has considerably more contrast compared to the carbonaceous capping agents. Low-contrast carbon-rich capping agents can be quite challenging to visualize without employing advanced techniques such as negative staining or low voltage TEM; therefore, reported electron microscopy sizes typically represent the core particle and ignore the size of any organic capping layer or other molecules associated with the AgNP that would increase in the hydrodynamic diameter. This is why TEM and AFM sizes often converge more closely than DLS with either form of microscopy.

AFM quantitatively measures the height of the AgNP. However, the dehydrated capping agent layer may or may not be included in the reported size, depending on the contact forces used during imaging. This effect is possible in the most common imaging modes, either in contact mode or intermittent contact (tapping) mode. In contact mode, loosely bound capping agent molecules may be physically scraped off the AgNP surface, while in intermittent contact mode, the force of the tip contacting the surface at the bottom of each "tap" may be sufficient to partially or completely indent through a compliant top layer of capping agents. Also, some capping agent molecules may decrease in size when solvent molecules associated with their most stable structure in solution are evaporated.[43] However, in many cases the contribution to the measured height from the capping layer is negligible relative to the core particle height.

AFM can provide topographical images, but the horizontal dimensions are difficult to quantify due to tip-broadening effects arising from the radius of curvature of the AFM tip, which can be compensated for through measurements of a size standard and a straightforward equation.[44] Moreover, for faceted particles (common for gold and AgNPs) the maximum height may be affected by the manner in which the facets are oriented with respect to the underlying substrate, and the measured *Z*-height of the NP may not reflect the maximum dimension of the nanoparticle if any spherical asymmetry exists.

One great advantage of AFM is the sub-nm resolution of *Z*-height measurements in a well-calibrated system, enabling confidence in measurements of very small (<5 nm) AgNPs. A word of caution is warranted when preparing histograms from AFM images. Various image output settings can make very small NPs appear either visually striking or nearly invisible (see Fig. S1 and S2† for details), running the risk of unintentional omissions when preparing a histogram and limiting one of the advantages of AFM. This risk is greatest when the difference between the diameter of the small and large NP populations is greatest. One example of this AFM advantage is illustrated in Fig. 3h, where the AFM measurements were able to observe a substantial population of very small AgNPs that are apparently "invisible" to the TEM and USAXS. While the AFM measurements alone,

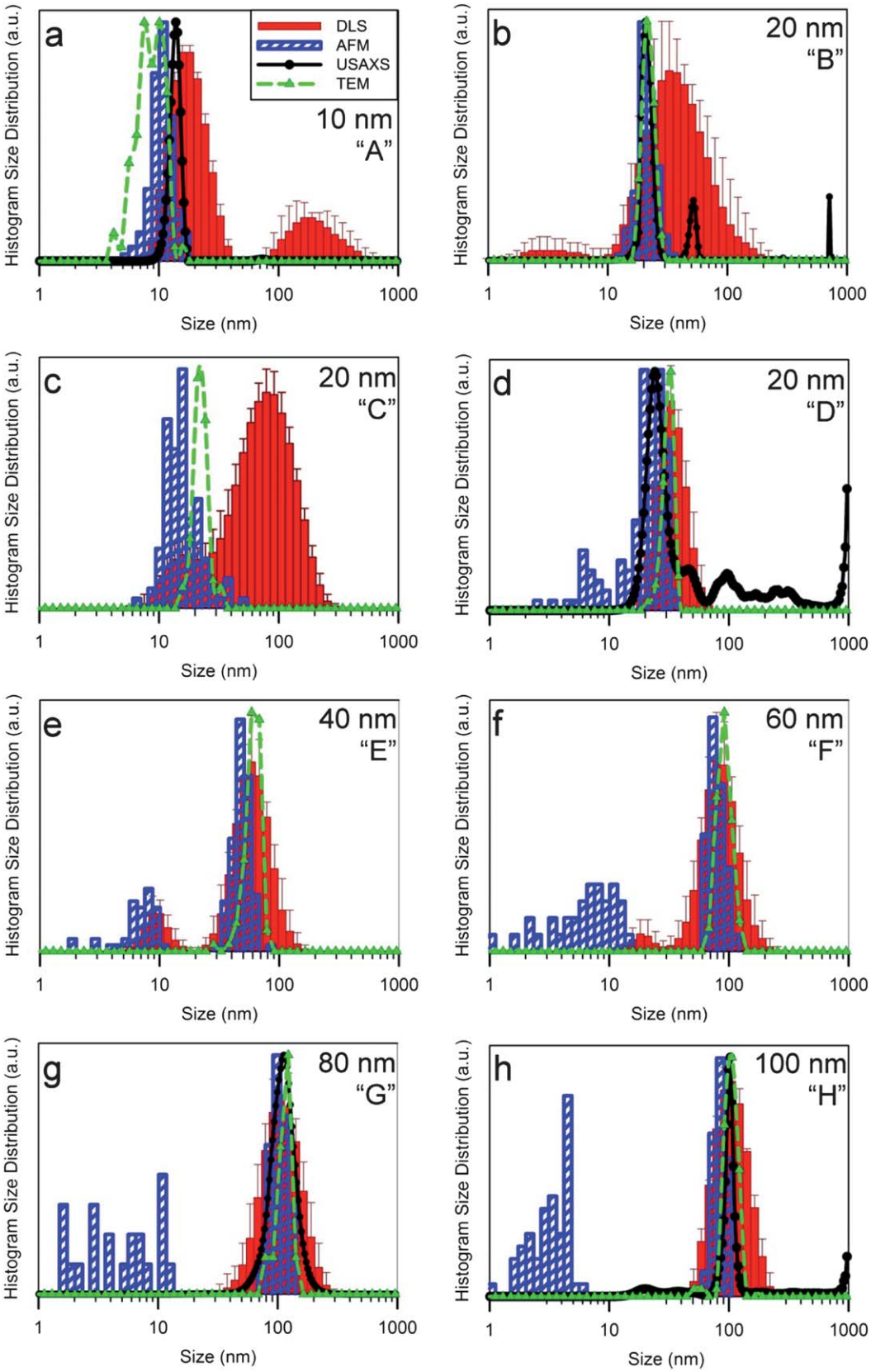

Fig. 3 Histogram size distributions of citrate-capped AgNPs under pristine conditions. DLS intensity-based size distributions (percent of total intensity signal), AFM particle heights (number of AgNPs counted), TEM particle diameters (number of AgNPs counted), and USAXS volume fraction histogram for citrate-capped AgNPs corresponding to Table 1 Samples A–H, respectively. All bin widths are logarithmically scaled to facilitate comparison.

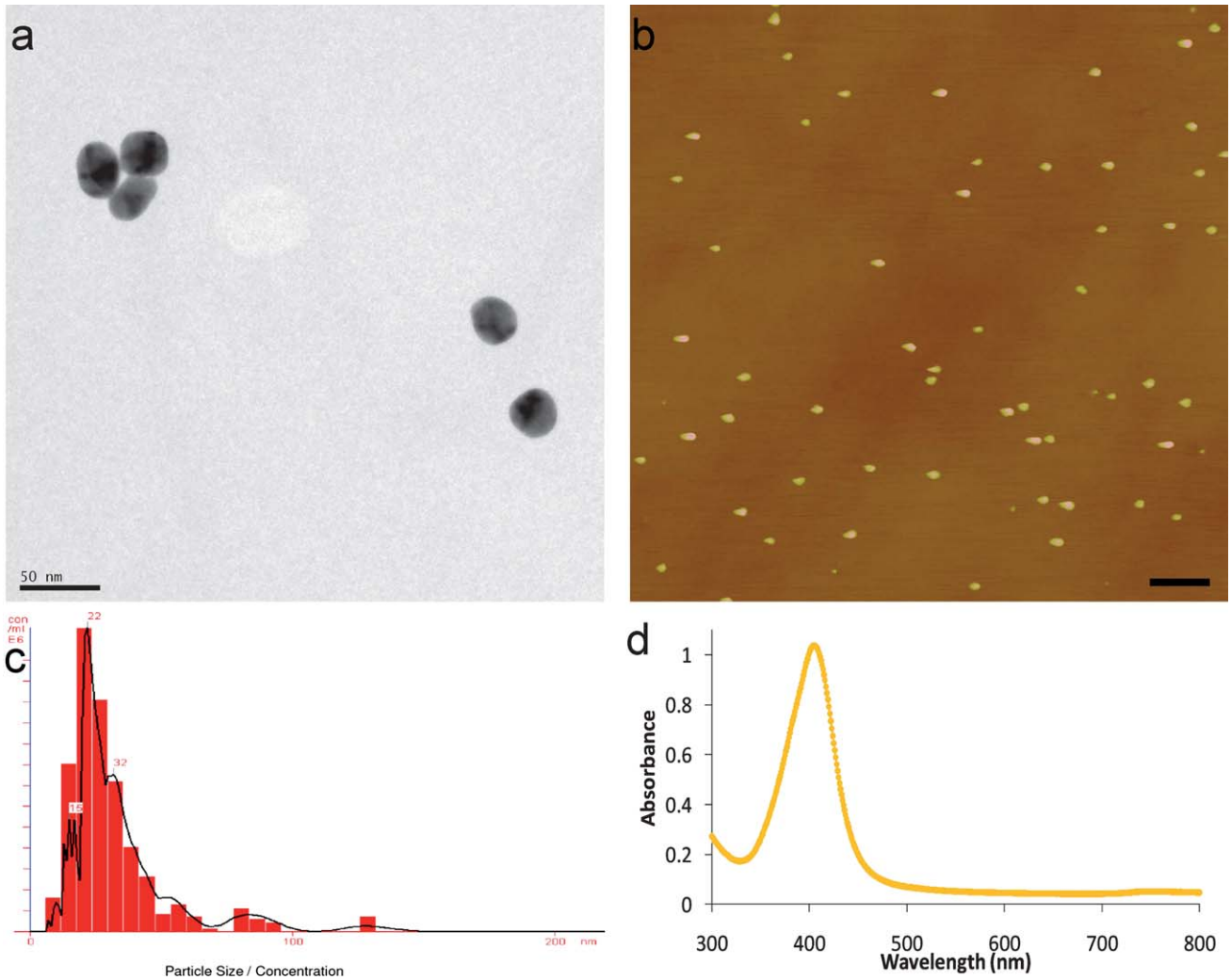

Fig. 4 Sample D, citrate-capped nominally 20 nm AgNPs, representative (a) TEM and (b) AFM images, (c) example size distribution from NTA data with over 100 completed tracks, and (d) UV-vis spectrum. Scale bars are (a) 50 nm and (b) 200 nm.

although convincing, do not prove the presence of the AgNPs, due to the challenges of distinguishing low concentrations of very small particles in mixtures with larger AgNPs by TEM and USAXS, these small particles cannot be treated as AFM artifacts either. Thus, a quick examination for very small AgNPs is suggested when preparing a size distribution by AFM, especially when reporting the sizes of materials used in hypothesis testing of size-based effects.

Further discussion on the reporting of uncertainties is warranted. The reported values from microscopy-based measurements are often the mean of all observed particles with one or two standard deviations about this mean (assumes a Gaussian distribution). The uncertainty in this case primarily reflects the width of the size distribution itself. The uncertainty in the mean of number-based particle sizing measurements (including NTA) can be reduced by increasing the number of particles sampled (*i.e.*, uncertainty is inversely proportional to the square of the particles counted). This is described in detail in NIST special publication 960-1.[45] On the other hand, DLS hydrodynamic measurements typically report the mean of several measurements performed under repeatability conditions with an uncertainty of one or two standard deviations about the mean of those measurements. For this case, the uncertainty represents the repeatability or precision of the mean size determination, and does not reflect the width of the particle distribution. This is an important distinction to keep in mind when comparing results across measurement methods.

Absorbance. Through the SPR absorbance of AgNPs, UV-vis spectroscopy can provide qualitative information about the size and size distribution, as well as quantitative information about their concentration. The SPR absorbance peak will be fairly narrow and centered close to a λ_{max} of 390 nm for AgNPs up to about 10 nm in diameter.[46] As the diameter increases, the SPR peak begins to broaden, and the λ_{max} wavelength begins to red-shift (see, for example, Fig. S27†).[47,48] NP shape asymmetry or coupling of the SPR across multiple NPs through agglomeration can induce either similar effects,[49,50] as well as broad, multiple or asymmetric peaks.[50,51] Additionally, SPR λ_{max} wavelengths and extinction coefficients are affected by the local dielectric environment surrounding the AgNP; consequently, changes to the electrolyte composition or concentration of the suspending

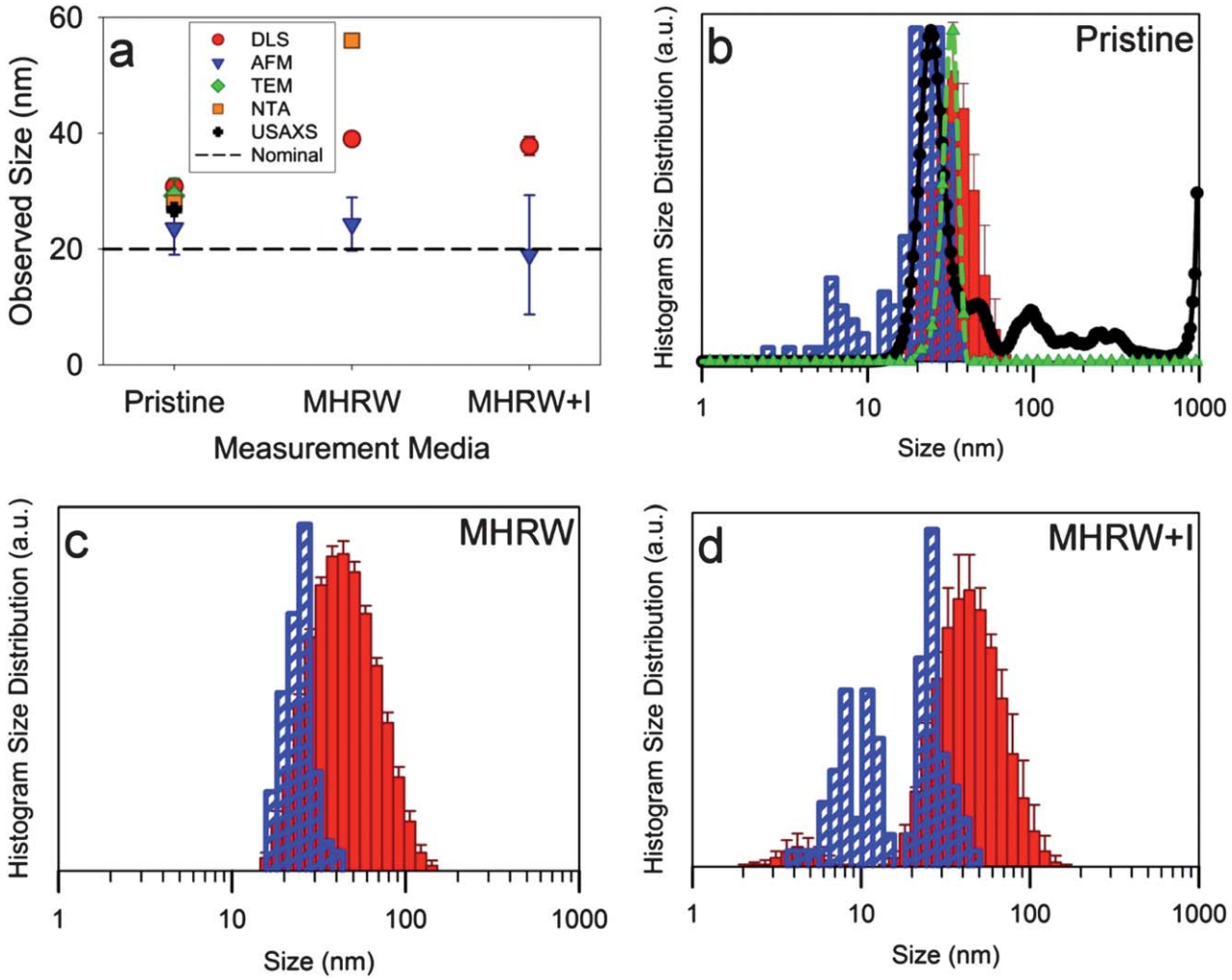

Fig. 5 (a) Observed mean size by measurement technique, plotted as a function of process steps or media conditions under which measurements of "stock" solutions could occur. Histogram size distributions for measurements under (b) pristine conditions, (c) MHRW, and (d) MHRW with NOM Standard I. Color scheme of legend in (a) applies to all panels. All data are from Sample D (nominally 20 nm citrate-capped AgNPs). See Tables 1–3 for uncertainties smaller than symbol size.

media, or changes to the surface chemistry or coating molecules, can alter λ_{max} to varying degrees.[49,52]

Hydrodynamic diameter measurement. DLS and NTA measure the hydrodynamic diameter of AgNPs *in situ*, which includes the Ag core, capping agents and any other molecules sorbed to the surface, and layers of solvent molecules that are associated with the NP during Brownian motion. These components are contained within a hydrodynamic sheath that is assumed to conform to a spherical geometry. Additionally, any agglomerates or aggregates present in the suspension will be measured and contribute to the mean size and polydispersity. Due to the fundamental metrology of DLS measurements, Raleigh scattering dictates that the light intensity scattered by a NP is proportional to its diameter raised to the sixth power, and thus larger diameter particles will dominate the intensity signal. Recently, Tsai *et al.*[53] reported an approach to estimate the contribution to the overall DLS intensity signal in a mixture of two types of NPs. To quantify the impact, these authors defined a dimensionless parameter

$$\gamma = \frac{\text{NP1 scattering intensity}}{\text{NP2 scattering intensity}} = \frac{\varepsilon_{NP1} N_{NP1} {d_{NP1}}^6}{\varepsilon_{NP2} N_{NP2} {d_{NP2}}^6}$$

where ε, N, and d are the refractive index, number concentration, and hydrodynamic diameters, respectively, with subscripts NP1 and NP2 indicating NP types 1 and 2, respectively. Assuming NP1 is larger than NP2, and similar values for ε and N for both NPs, an increase in γ will reflect the decreased contribution from NP2 (here, the smaller NP) on the observed DLS scattering intensity. For example, if there was an equal number of 5 nm and 50 nm AgNPs in a mixture, then γ would be 10^6. This is a plausible situation that might occur, for instance, if a selective dissolution process was occurring to only a fraction of AgNPs in a sample.

NTA measures the Brownian motion of individual AgNPs by tracking the two-dimensional projection of their three-dimensional motion *via* collections of diffraction image videos using a CCD detector. The NTA manufacturer's proprietary software determines the location in the field of view of the center of the spot of light scattered by a single NP. Since the distance between

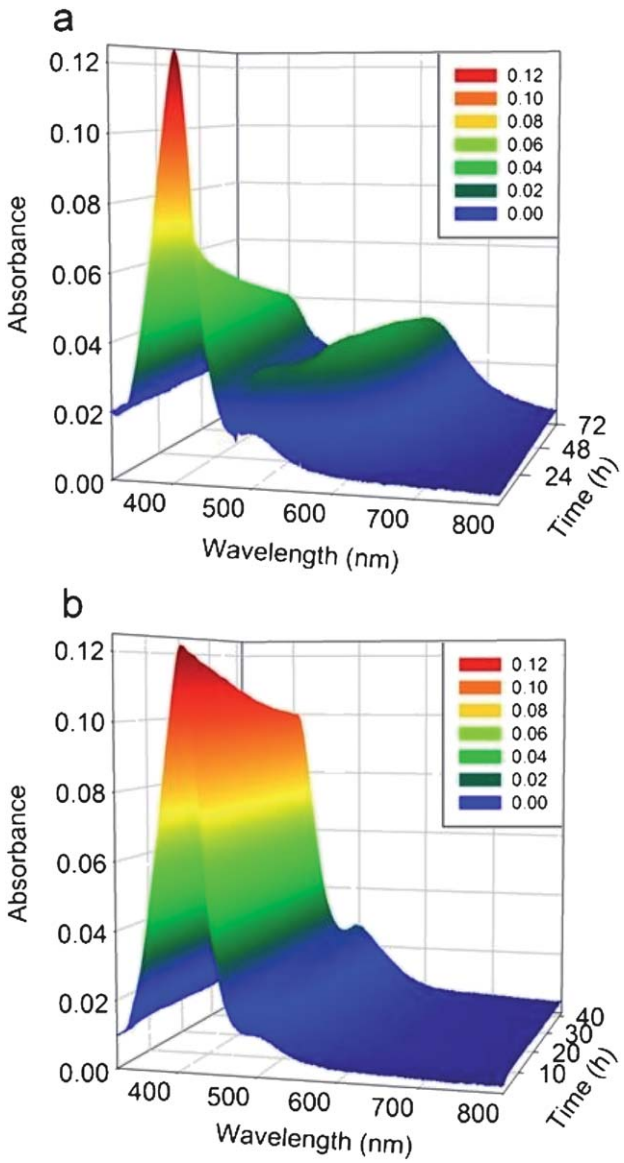

Fig. 6 UV-vis absorbance spectra over time for Sample D, citrate-capped nominally 20 nm AgNPs, diluted into (a) MHRW with NOM Standard I and (b) MHRW with NOM Standard II. False colors (legend inset) represent the absorbance intensity. Spectra were collected every 1 h for 72 h in (a) and 42 h in (b).

pixels and time between frames are known, the velocity of the center spot is calculable, and the Brownian motion and hydrodynamic diameter can thus be calculated. Because NTA is tracking individual scatterers, the method is not as subject to the γ intensity limitations of DLS when measuring polydisperse samples. Rather, the relative intensity (*i.e.*, pixel brightness) is recorded in addition to the hydrodynamic diameter, allowing a user to determine if there are multiple populations of NPs with the same hydrodynamic radius but different refractive indices. This is similar to comparing the relative contrast by TEM of similar sized NPs composed of, for instance, different elements, and is something DLS cannot do. NTA is also capable of measuring hundreds of individual AgNPs in much less time than required by microscopy techniques and reports both the mean and mode hydrodynamic diameter. Nevertheless, NTA is also subject to certain limitations.[54] Due to laser power and camera detector limitations, particles with diameters less than about 40 nm become increasingly challenging to measure with the systems employed in the present work; below about 20 nm reliable data cannot be obtained. Also, the concentration ranges of this technique are narrowly limited. A sufficient number of NPs must be in the field of view to obtain a meaningful number of completed tracks, typically at least 300, in a reasonably short time, yet there must not be so many particles that they cross paths so frequently that the software cannot distinguish each NP's trajectory from frame to frame.

USAXS

USAXS, like electron microscopy, provides greater contrast with increasing atomic number. Synchrotron based measurements in liquid cells enable size and size distribution measurements of the Ag core of the AgNP under *in situ* conditions,[55] and in certain cases the ability to measure when AgNPs are in close and ordered proximity to each other, from dimers to agglomerates up to colloidal crystals. See the ESI† (Fig. S3) for extended discussion on the importance of careful background subtraction in USAXS samples with low scattering intensity, a scenario that is likely to be encountered at environmentally relevant concentrations, but which can sometimes be overcome.

Additionally, calibrated USAXS has the capacity to resolve mean, median, or mode diameters for each population in a multimodal size distribution, on a quantitative basis, yielding volume fraction (*i.e.*, concentration) of scatterers (*i.e.*, AgNPs) in solution contributing to each part of that specific distribution. Quantitative USAXS results involve instrumental calibration by direct beam intensity measurement. USAXS also works well for resolving multiple populations in close size proximity, unlike DLS which requires separation of population sizes by at least a factor of three.

Challenges comparing size and size distribution results

When considered collectively, the six techniques described above can provide the sizes and size distributions of the Ag core, Ag core plus hydrated organic shell (in solution), and Ag core plus dehydrated shell (in air). This range of information presents both challenges and opportunities. For example, it is problematic and not uncommon that the same AgNPs can be reported to have significantly different sizes or size distributions; this is especially true if separate groups of investigators rely upon a single technique to report size. However, a strategic selection of measurement approaches applied to the same sample can provide information about size, size distribution, agglomeration state and organic shell coating thickness, information not obtainable from a single technique.

Comparison of the results from Table 1 for Sample D, nominally 20 nm citrate-capped AgNPs, indicates how differences in measurement methods manifest themselves in the experimental data. The measured mean diameters are 30.8 ± 1.2 nm for DLS, 29.2 ± 3.0 nm for TEM, 28 nm for NTA, 27.9 ± 2.8 nm for the USAXS primary population, and (23.6 ± 4.6) nm for AFM, keeping in mind the differences in uncertainties across techniques

described earlier. Based on results reported for citrate-capped gold NPs under pristine conditions,[35] a 5 nm spread in mean size between several techniques for the same sample is a reasonable expectation. In that context, a 7 nm difference for AgNPs does not seem unreasonable, assuming a similar size distribution. Moreover, DLS, as expected, yields the largest apparent size, and AFM yields the smallest. The same trend was reported for citrate-capped gold NPs, including the close correlation between USAXS and AFM.

To some extent these observed trends can be related to the different ways in which the analyses are weighted. Different techniques commonly report different bases for size distributions. For example, ASTM standard E2490-09 recommends that the native intensity-based size distribution be reported for DLS measurements, which is equivalent to a volume-squared-basis for NPs. For USAXS, the volume- or mass-based size distribution is typically reported, while NTA, AFM and TEM generate number-based size distributions. Techniques that report higher moments of the distribution (*e.g.*, DLS Z_{avg}) will yield mean sizes that are generally larger for the same particle population; the broader the distribution, the greater the spread in mean size values. Moreover, converting from number-based to volume-based to volume-squared-based will lead to a progressively diminishing contribution from the smallest diameter NPs. Inversely a very small amount of noise, error or uncertainty in the data could be magnified to an incorrect over-representation of small NPs in a calculated volume-based distribution from a volume-squared-based distribution. For example, converting from a number basis to a volume basis, a single 100 nm AgNP would occupy the same volume as 10^6 1 nm AgNPs; it would be extremely challenging in an experimental setting to achieve precision and accuracy to well beyond six significant figures for any technique (*e.g.*, sizing over one million AgNPs by microscopy). Therefore, while these conversions may be theoretically valid, they are mathematically ill-posed and not recommended (*e.g.*, see ASTM E2490-09). Thus, extreme care must be taken before a claim about monodispersity can be made using any single technique, or when comparing results from two techniques with different bases.

Fig. 3 compares the size distributions of various citrate-capped AgNP suspensions under pristine conditions by DLS, USAXS, TEM and AFM measurements, and provides examples of each of three bases for size distribution. In Fig. 3, the bins have been adjusted from their typical presentation styles to create size distribution graphs with bin widths that are equivalent across the different measurement methods.

Fig. 3a shows the size distributions for AgNPs with a reported nominal diameter of 10 nm (Sample A, Table 1). The mean diameter values and relative distributions as measured by TEM, AFM and USAXS are similar. For the DLS measurements, the mean hydrodynamic diameter value was larger and the particle population was more polydisperse, as an additional AgNP population was detected centered above 100 nm. Although the nominal diameters for the AgNPs in Fig. 3b–d are 20 nm, the samples have similar mean values but different size distributions as measured by AFM. Fig. 3e–h show size distributions for AgNPs with nominal diameters of 40, 60, 80, and 100 nm, respectively. For these AgNPs, the AFM measurements indicate a bimodal distribution with a population of larger particles corresponding to the nominal diameters and a population of smaller particles showing diameters less than 10 nm. In Fig. 3g–h, nominally the largest AgNP samples, AFM alone detects the presence of a very small diameter population of AgNPs, whereas the remaining techniques are in close alignment. The detected populations of small diameter (<10 nm) particles may have resulted from the AgNPs dissolving during the unknown total time between their manufacture and their receipt and imaging.[56–58] Alternatively, while it is not known precisely how the AgNPs were synthesized, seed-mediated growth methods are reported in the literature,[59] and it may be possible that some excess seeds did not react and were not subsequently removed.

Fig. 3 highlights the advantage and the importance of using multiple techniques to characterize and report the size of a nanomaterial. For example, by pairing DLS and AFM, a comparison of results across techniques improves understanding of the material's actual composition. For example, in Fig. 3h, assuming from the AFM size distribution that the population with the greatest number concentration of small NPs is 100 nm diameter AgNPs with approximately 60% of the observed particles being less than 10 nm, the difference in DLS intensity between populations, γ, would be on the order of 10^4. Similarly, for a case with a narrower bimodal distribution of sizes by AFM (nominally 40 nm AgNPs, Fig. 3e), approximately 25% of the observed particles are less than 10 nm and approximately 75% are in a population with an average of 48 nm, resulting in γ on the order of 10^3. Thus, it is not surprising that DLS detects agglomeration that AFM misses, and, *vice versa*, that AFM can see extremely small AgNPs to which DLS is insensitive. Therefore, the great benefit of pairing DLS with AFM is revealed.

Also, it is important to note that, for multimodal distributions of NP size, the average size of all AgNPs observed in a number distribution may not be the most informative way to report the size. It is recommended to report the full size distribution whenever possible. Identification of the mean or mode of each peak in the size distribution may be more appropriate, as highlighted by the distributions shown in Fig. 3 and the mean diameter values given in Table 1. For example, Sample H (citrate-capped nominally 100 nm) has two populations in the AFM size distribution, the first with a mean size of 3.3 ± 1.2 nm and a second (principal population) of 83.7 ± 8.8 nm. The overall mean particle size observed by AFM is 39.5 ± 40.6 nm, a particle size that does not actually exist in this distribution. Since the DLS Z_{avg} size is 98.7 ± 1.2 nm, if one were to report only the second population from the AFM size distribution (either intentionally or unintentionally), the AFM and DLS results would be in apparent agreement, though omitting a potentially important fraction of the dispersion. From a biological perspective, when attempting to assess the risk of a specific size NP crossing certain biological barriers, or the available AgNP surface area per unit volume of solution, the small AgNPs in Sample H may become critical to successful interpretation of data.

Although beyond the scope of the present work, it is worth noting that the application of chromatographic separation methods coupled with size measurement or particle counting detectors can yield more definitive results with respect to assessing materials with multiple populations, and can help to rule out common artifacts. Such approaches include size

exclusion chromatograpy,[60] dynamic mobility analysis (aerosol based),[43,53] and field flow fractionation.[61]

Recommendations

The accurate reporting of the size and size distribution of AgNPs in test media is critical to the successful intercomparison of reported size results and to the proper interpretation of environmental and biological fate assessments. Assigning a value based on the application of a single measurement technique is generally not the best approach. Selection of multiple measurement tools that provide orthogonal or complementary size information (such as hydrodynamic diameter and hard core diameter) is critical to not only reducing the risk of missing an observation that may later prove important but also in facilitating comparison of reported results. There is currently no one single technique available that can effectively capture all of the important and relevant information needed to report NP size and size distributions. However, the judicious selection of a set of techniques can be used to validate routine lower-cost and higher-throughput "screening" characterization. Collaboration between interdisciplinary expert groups can help facilitate and expedite this important initial phase of research projects. This routine screening can be an effective way to assure that multiple preparations of AgNPs throughout a systematic study have acceptably minimal variation, and thereby (for example) consistent dosing of aquatic organisms or cell cultures. Selection of the appropriate pre-screening techniques depends upon the specific system of interest, *i.e.* there is no universal single best measurement method or combination of methods. However, once a detailed understanding is achieved, rational selection of the best approach with tolerable uncertainties for routine experimental dosing quality control should become obvious to the practitioner. An example process flow may be as follows:

1. Apply available orthogonal measurement techniques, both intensive and routine, to thoroughly characterize materials initially under experimental process conditions, also checking for changes over the time-frame of experiments.

2. Identify deviations (changes in size, concentration, agglomeration state, *etc.*) that may indicate an unacceptable change in properties of the material.

3. Identify and determine the minimum number of routine techniques required to best identify those deviations once baseline data have been established.

4. Investigate further whenever unexpected results occur (either through routine AgNP monitoring or the process or test under development performs unexpectedly).

For example, imagine an assay conducted in a laboratory reconstituted environmental water system. By characterizing the NPs to be studied under the exact procedures, conditions, and times in a detailed fashion before introduction into environmental assays, a collaborative research team may develop a map of the agglomeration state of the NPs over the time of the experiment using several techniques. The team might then determine that UV-vis spectroscopy combined with DLS would be an acceptable way of routinely monitoring for unexpected events (*e.g.*, changes in agglomeration state). While experiments (*e.g.*, aquatic organism toxicity) are running, the actual batches of NPs used in the environmental media may then be monitored *ex situ* by UV-vis and DLS. If the assay provides anomalous or unexpected results, or if either the UV-vis or DLS measurements deviate from baseline values, then the team might investigate the origins of these results using non-routine approaches.

While the present work has focused more on dimensional characterization of AgNPs, of equal or greater importance to many nanoEHS risk assessment models is quantifying the various species of silver in the system (*e.g.*, AgNP, Ag(I), Ag_2O or Ag_2S shell layers on the AgNPs, *etc.*).[57,62] Similar to reporting size results, great care must be employed in measuring, reporting, and comparing these chemical results.

Maximum transparency is required in reporting size and size distributions from multiple orthogonal measurement techniques. While many journals strive to achieve minimum word counts on the main text of articles, there are often no such limitations to the use and length of ESI†. Therefore, the authors recommend including as many details of the physico-chemical characterization of NP stocks as is practically possible in the ESI† of a manuscript, to both strengthen the quality of the conclusions drawn and to have a greater impact on advancing the knowledge of the field. Due to the dynamic, intrinsically unstable nature of AgNPs that makes them challenging to study, there are experimental details beyond those typically cited in "minimum characterization" lists that may have previously been considered trivial but should, if possible, be reported in the future, including:

- Size distributions (*e.g.*, histograms) from multiple orthogonal measurement techniques.
- Detailed specification of "stock" characterization media and processing.
- Time elapsed between synthesis, dispersion preparation, size distribution measurements, and final experiments.
- Identification if different batches were used in initial stability characterization and final experiments, and batch-to-batch variation observed in AgNP stocks.
- How routine screening or quality control checks were initially validated, and subsequently used throughout the studies.
- Duplicate microscopy images representative of those used to create histograms, one optimized to ensure small NPs (less than 5 nm) were not omitted, and one optimized for the larger "primary" particle size.

Reporting these details routinely will facilitate the intercomparison of results across reports, allowing detailed understanding of what is truly meant by the nominal value of the AgNPs employed in any given experiment. While in situations with narrow monomodal size distributions convergence of the mean size across techniques and conditions should be observed, in our experience few commercial or laboratory-prepared AgNPs will actually yield such results.

Conclusion

Detailed reporting of physical characterization of AgNPs using multiple, orthogonal measurement techniques will facilitate the intercomparison of environmental risk assessment findings from different laboratories and improve confidence in results. Improved sharing of results can contribute to more rapid understanding of the overall fate, transformations, and potential hazards of AgNPs in the environment, allowing more confidence for nanoEHS risk assessment.

Disclaimer

Certain trade names and company products are mentioned in the text or identified in illustrations in order to specify adequately the experimental procedure and equipment used. In no case does such identification imply recommendation or endorsement by the National Institute of Standards and Technology or the US Environmental Protection Agency, nor does it imply that the products are necessarily the best available for the purpose.

Acknowledgements

The use of the Advanced Photon Source at Argonne National Laboratory was supported by the U.S. Department of Energy, Office of Science, Office of Basic Energy Sciences, under contract no. DE-AC02-06CH11357. ChemMatCARS Sector 15 is principally supported by the National Science Foundation/Department of Energy under grant number CHE-0535644. Dr Jan Ilavsky, X-ray Science Division, and Dr Yu-Sheng Chen, ChemMatCARS, both from the Advanced Photon Source, are acknowledged for assistance with measurements. M.N.M. acknowledges support under the NIST American Recovery and Reinvestment Act Measurement Science and Engineering Fellowship Program Award 70NANB10H026 through the University of Maryland.

References

1 D. C. Tien, K. H. Tseng, C. Y. Liao, J. C. Huang and T. T. Tsung, *J. Alloys Compd.*, 2008, **463**, 408–411.
2 S. Luoma, *Project on Emerging Nanotechnologies 15-Silver Nanotechnologies and the Environment*, 2008, http://www.nanotechproject.org/publications/archive/silver/.
3 S. W. P. Wijnhoven, W. J. G. M. Peijnenburg, C. A. Herberts, W. I. Hagens, A. G. Oomen, E. H. W. Heugens, B. Roszek, J. Bisschops, I. Gosens, D. Van De Meent, S. Dekkers, W. H. De Jong, M. van Zijverden, A. n. J. A. M. Sips and R. E. Geertsma, *Nanotoxicology*, 2009, **3**, 109–138.
4 V. K. Sharma, R. A. Yngard and Y. Lin, *Adv. Colloid Interface Sci.*, 2009, **145**, 83–96.
5 M. R. Wiesner, G. V. Lowry, P. Alvarez, D. Dionysiou and P. Biswas, *Environ. Sci. Technol.*, 2006, **40**, 4336–4345.
6 B. Erickson, *Chem. Eng. News*, 2009, **87**, 25–26.
7 US Environmental Protection Agency, 2009 http://www.epa.gov/scipoly/sap/meetings/2009/november/110309ameetingminutes.pdf.
8 US Food and Drug Administration, 2007, http://www.fda.gov/AboutFDA/CentersOffices/CDRH/CDRHReports/ucm126688.htm.
9 L. S. Wen, P. H. Santschi, G. A. Gill, C. L. Paternostro and R. D. Lehman, *Environ. Sci. Technol.*, 1997, **31**, 723–731.
10 J. A. Gomez-Caballero, M. G. Villasenor-Cabral, P. Santiago-Jacinto and F. Ponce-Abad, *Can. Mineral.*, 2010, **48**, 1237–1253.
11 R. I. MacCuspie, *J. Nanopart. Res.*, 2011, DOI: 10.1007/s11051-010-0178-x.
12 J. Gao, S. Youn, A. Hovsepyan, V. ü. L. Llaneza, Y. Wang, G. Bitton and J. C. Bonzongo, *Environ. Sci. Technol.*, 2009, **43**, 3322–3328.
13 I. Lynch and K. A. Dawson, *Nano Today*, 2008, **3**, 40–47.
14 T. M. Sager, D. W. Porter, V. A. Robinson, W. G. Lindsley, D. E. Schwegler-Berry and V. Castranova, *Nanotoxicology*, 2007, **1**, 118–129.
15 S. Harper, C. Usenko, J. E. Hutchison, B. L. S. Maddux and R. L. Tanguay, *J. Exp. Nanosci.*, 2008, **3**, 195–206.
16 M. R. Wiesner, G. V. Lowry, K. L. Jones, M. F. Hochella, R. T. Di Giulio, E. Casman and E. S. Bernhardt, *Environ. Sci. Technol.*, 2009, **43**, 6458–6462.
17 R. I. MacCuspie, A. M. Elsen, S. J. Diamanti, S. T. Patton, I. Altfeder, J. D. Jacobs, A. A. Voevodin and R. A. Vaia, *Appl. Organomet. Chem.*, 2010, **24**, 590–599.
18 E. Navarro, A. Baun, R. Behra, N. B. Hartmann, J. Filser, A. J. Miao, A. Quigg, P. H. Santschi and L. Sigg, *Ecotoxicology*, 2008, **17**, 372–386.
19 T. M. Tolaymat, A. M. El Badawy, A. Genaidy, K. G. Scheckel, T. P. Luxton and M. Suidan, *Sci. Total Environ.*, 2010, **408**, 999–1006.
20 S. Elzey and V. Grassian, *J. Nanopart. Res.*, 2010, **12**, 1945–1958.
21 V. Filipe, A. Hawe and W. Jiskoot, *Pharm. Res.*, 2010, **27**, 796–810.
22 USEPA, *Methods for Measuring the Acute Toxicity of Effluents and Receiving Waters to Freshwater and Marine Organisms*, 821/R-02–012, 2002.
23 V. A. Hackley and J. D. Clogston, *Measuring the Size of Nanoparticles in Aqueous Media Using Batch-Mode Dynamic Light Scattering*, NIST-NCL Assay Protocol PCC-1, 2007, http://ncl.cancer.gov/working_assay-cascade.asp.
24 J. E. Bonevich and W. K. Haller, *Measuring the Size of Nanoparticles Using Transmission Electron Microscopy*, NIST-NCL Assay Cascade Protocol PCC-7, 2010, http://ncl.cancer.gov/working_assay-cascade.asp.
25 M. D. Abramoff, P. J. Magelhaes and S. J. Ram, *Biophotonics International*, 2004, **11**, 36–42.
26 W. S. Rasband, *ImageJ*, 1997, http://rsb.info.nih.gov/ij/.
27 J. Grobelny, F. W. Delrio, N. Pradeep, D.-I. Kim, V. A. Hackley, and R. F. Cook, *Size Measurement of Nanoparticles Using Atomic Force Microscopy*, NIST-NCL Assay Cascade Protocol PCC-6, 2009, http://ncl.cancer.gov/working_assay-cascade.asp.
28 Research Report E56-1001, *Interlaboratory Study to Establish Precision Statements for ASTM E2490-09 Standard Guide for Measurement of Particle Size Distribution of Nanomaterials in Suspension by Photon Correlation Spectroscopy*, 2009.
29 A. J. Allen, V. A. Hackley, P. R. Jemian, J. Ilavsky, J. M. Raitano and S. W. Chan, *J. Appl. Crystallogr.*, 2008, **41**, 918–929.
30 D. J. Cookson, N. Kirby, R. Knott, M. Lee and D. Schultz, *J. Synchrotron Radiat.*, 2006, **13**, 440–444.
31 J. Ilavsky, P. R. Jemian, A. J. Allen, F. Zhang, L. E. Levine and G. G. Long, *J. Appl. Crystallogr.*, 2009, **42**, 469–479.
32 J. A. Lake, *Acta Crystallogr.*, 1967, **23**, 191–194.
33 J. A. Potton, G. J. Daniell and B. D. Rainford, *J. Appl. Crystallogr.*, 1988, **21**, 663–668.
34 J. Ilavsky and P. R. Jemian, *J. Appl. Crystallogr.*, 2009, **42**, 347–353.
35 *Reference Material 8011, Gold Nanoparticles Nominally 10 nm, Report of Investigation*, National Institute of Standards and Technology, Gaithersburg, MD, 2008, http://www.nist.gov/srm/.
36 *Reference Material 8012, Gold Nanoparticles Nominally 30 nm, Report of Investigation*, National Institute of Standards and Technology, Gaithersburg, MD, 2008, http://www.nist.gov/srm/.
37 *Reference Material 8013, Gold Nanoparticles Nominally 60 nm, Report of Investigation*, National Institute of Standards and Technology, Gaithersburg, MD, 2008, http://www.nist.gov/srm/.
38 J. T. Taurozzi, V. A. Hackley and M. R. Wiesner, *Nanotoxicology*, 2011, DOI: 10.3109/17435390.2010.528846.
39 J. T. Taurozzi, V. A. Hackley and M. R. Wiesner, *CEINT-NIST Protocol*, 2010, 1, 1–10, http://www.ceint.duke.edu/allprotocols.
40 J. T. Taurozzi, V. A. Hackley and M. R. Wiesner, CEINT-NIST Protocol, 2010, **2**, 1–5, http://www.ceint.duke.edu/allprotocols.
41 C. L. A. Geronimo and R. I. MacCuspie, *Microsc. Microanal.*, 2011, **17**, DOI: 10.1017/S1431927610094559.
42 R. I. MacCuspie, I. A. Banerjee, C. Pejoux, S. Gummalla, H. S. Mostowski, P. R. Krause and H. Matsui, *Soft Matter*, 2008, **4**, 833–839.
43 D.-H. Tsai, F. W. DelRio, R. I. MacCuspie, T. J. Cho, M. Zachariah and V. A. Hackley, *Langmuir*, 2010, **26**, 10325–10333.
44 P. Markiewicz and M. C. Goh, *Langmuir*, 1994, **10**, 5–7.
45 A. Jillavenkatesa, S. J. Dapkunas, and L.-S. H. Lum, *Particle Size Characterization - NIST Recommended Practice Guide, Special Publication 960–1*, 2001.
46 S. Link and M. A. El-Sayed, *J. Phys. Chem. B*, 1999, **103**, 8410–8426.
47 D. D. Evanoff and G. Chumanov, *ChemPhysChem*, 2005, **6**, 1221–1231.
48 D. D. Evanoff and G. Chumanov, *J. Phys. Chem. B*, 2004, **108**, 13957–13962.
49 J. Duan, K. Park, R. I. MacCuspie, R. A. Vaia and R. Pachter, *J. Phys. Chem. C*, 2009, **113**, 15524–15532.

50 J. M. Zook, R. I. MacCuspie, L. E. Locascio, M. D. Halter and J. E. Elliott, *Nanotoxicology*, 2011, DOI: 10.3109/17435390.2010.536615.
51 R. Elghanian, J. J. Storhoff, R. C. Mucic, R. L. Letsinger and C. A. Mirkin, *Science*, 1997, **277**, 1078–1081.
52 M. D. Malinsky, K. L. Kelly, G. C. Schatz and R. P. Van Duyne, *J. Am. Chem. Soc.*, 2001, **123**, 1471–1482.
53 D.-H. Tsai, F. W. DelRio, A. M. Keene, K. M. Tyner, R. I. MacCuspie, T. J. Cho, M. R. Zachariah and V. A. Hackley, *Langmuir*, 2011, **27**, 2464–2477.
54 V. Filipe, A. Hawe and W. Jiskoot, *Pharm. Res.*, 2010, **27**, 796–810.
55 R. I. MacCuspie, A. J. Allen and V. A. Hackley, *Nanotoxicology*, 2011, DOI: 10.3109/17435390.2010.504311.
56 J. Liu and R. H. Hurt, *Environ. Sci. Technol.*, 2010, **44**, 2169–2175.
57 J. Liu, D. A. Sonshine, S. Shervani and R. H. Hurt, *ACS Nano*, 2010, **4**, 6903–6913.
58 J. G. Gorham, R. I. MacCuspie, R. D. Holbrook and D. H. Fairbrother, *Environ. Sci. Technol.*, 2011, unpublished work.
59 G. Frens, *Nature (London), Phys. Sci.*, 1973, **241**, 20–22.
60 X. Y. Shi, I. J. Majoros, A. K. Patri, X. D. Bi, M. T. Islam, A. Desai, T. R. Ganser and J. R. Baker, *Analyst*, 2006, **131**, 374–381.
61 T. J. Cho and V. A. Hackley, *Anal. Bioanal. Chem.*, 2010, **398**, 2003–2018.
62 A. J. Kennedy, M. S. Hull, A. J. Bednar, J. D. Goss, J. C. Gunter, J. L. Bouldin, P. J. Vikesland and J. A. Steevens, *Environ. Sci. Technol.*, 2010, **44**, 9571–9577.

